Bio-Design and Manufacturing (2024) 7:597–610
https://doi.org/10.1007/s42242-024-00315-0

RESEARCH ARTICLE

Temporal and spatial regulation of biomimetic vascularization in 3D-printed skeletal muscles

Minxuan Jia[1,2,3] · Tingting Fan[1,2,3] · Tan Jia[2,3,4] · Xin Liu[1,2,3] · Heng Liu[1,5] · Qi Gu[1,2,3]

Received: 30 September 2023 / Accepted: 19 August 2024 / Published online: 26 September 2024

Abstract

In the intricate skeletal muscle tissue, the symbiotic relationship between myotubes and their supporting vasculature is pivotal in delivering essential oxygen and nutrients. This study explored the complex interplay between skeletal muscle and endothelial cells in the vascularization of muscle tissue. By harnessing the capabilities of three-dimensional (3D) bioprinting and modeling, we developed a novel approach involving the co-construction of endothelial and muscle cells, followed by their subsequent differentiation. Our findings highlight the importance of the interaction dynamics between these two cell types. Notably, introducing endothelial cells during the advanced phases of muscle differentiation enhanced myotube assembly. Moreover, it stimulated the development of the vascular network, paving the way for the early stages of vascularized skeletal muscle development. The methodology proposed in this study indicates the potential for constructing large-scale, physiologically aligned skeletal muscle. Additionally, it highlights the need for exploring the delicate equilibrium and mutual interactions between muscle and endothelial cells. Based on the multicell-type interaction model, we can predict promising pathways for constructing even more intricate tissues or organs.

Minxuan Jia, Tingting Fan, and Tan Jia have contributed equally to this work.

✉ Qi Gu
qgu@ioz.ac.cn

1 Key Laboratory of Organ Regeneration and Reconstruction, State Key Laboratory of Membrane Biology, Institute of Zoology, Chinese Academy of Sciences, Beijing 100101, China

2 Beijing Institute for Stem Cell and Regenerative Medicine, Beijing 100101, China

3 University of Chinese Academy of Sciences, Beijing 100049, China

4 State Key Laboratory of Stem Cell and Reproductive Biology, Institute of Zoology, Chinese Academy of Sciences, Beijing 100101, China

5 Department of Orthopaedics, Beijing Jishuitan Hospital, Capital Medical University, Beijing 100035, China

Graphic abstract

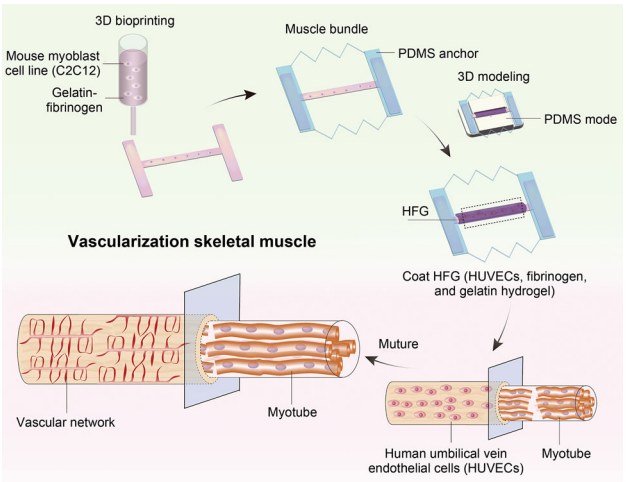

Keywords Skeletal muscle · Vascularization · 3D bioprinting · Cell interaction

Introduction

Approximately 85% of the skeletal muscle tissue comprises multinucleated myotubes, with the remaining 15% constituted by the nervous system, vasculature, and connective tissues [1–3]. Capillaries distributed around muscle bundles serve a dual purpose during skeletal muscle development. They are essential for supplying oxygen and nutrients and are pivotal in promoting the generation and repair of skeletal muscle tissue [4–6]. Following muscle injury, endothelial cells are known to be activated by biological and mechanical cues to form new vascular networks [7]. The interplay between the vascular network and muscle fibers is intimately linked, greatly influencing the injury repair process [8]. When the skeletal muscle defect exceeds 20%, it results in volumetric muscle defects [9]. Currently, the primary clinical treatment for these defects is autologous muscle transplantation; however, this approach has a high failure rate [10, 11]. With the advent of tissue engineering, novel avenues for clinical treatments include two-dimensional (2D) inoculation, three-dimensional (3D) replication, and 3D printing technology [11]. The partial functionalization and cell orientation of the skeletal muscle have been reported, and phased progress has been made in animal experiments. Thus, 3D printing has shown early success in the construction of vascularized skeletal muscles [12].

The skeletal muscle is rich in vasculature, with each myotube intricately surrounded by a capillary network [13]. To recreate skeletal muscle structures where blood vessels envelop myotubes, interventional engineering methods are of paramount importance. Understanding the vascular network formation in injured skeletal muscles necessitates the exploration of the interactions between capillaries and myotubes. Owing to their delicate structure and intimate association [8], constructing engineered vascularized skeletal muscles has become essential for accurately assessing the interplay between skeletal muscle myotubes and vascular endothelial cells [14]. From a biomimetic viewpoint, vascular network formation occurs synchronously with skeletal muscle tissue differentiation in vivo [7]. Thus, determining the optimal time for the vascularization of skeletal muscle tissue in vitro, understanding the temporal and spatial dynamics of the co-culture of multiple cells and crafting intricately structured vascularized skeletal muscle tissue are of crucial importance.

There is a refined methodology for in vitro skeletal muscle construction, which has enabled muscle vascularization. 3D printing was used to construct mature and oriented skeletal muscle, which can recover skeletal muscle function by 82% [15]. Fan et al. [16] used 3D bioprinting to construct skeletal muscle tissue and found that spatial constraints play an important role in the orientation differentiation of skeletal muscle. However, developing new tissue engineering techniques for crafting vascularized skeletal muscles suitable for in vivo transplantation and functional recovery is indispensable. Regarding cell orientation, the aligned microstructure can facilitate cellular cultivation and tissue transplantation [17]. Sequential modeling allows for tissue investigation in distinct tubes, emphasizing muscle cell–vascular endothelial cell interactions [8]. The mold can integrate cells within 3D hydrogels by co-culturing multiple cells, forming muscle bundles with vascular networks and motor neurons [18].

Significant advancements have been made recently in tissue engineering for the in vitro construction and animal

transplantation of vascularized skeletal muscles. For the construction of large-scale vascularized skeletal muscles, 3D sub-liquid coaxial printing was used to encapsulate muscle bundles within a vascular network structure. This approach indicated that up to 85% of the functional damage of volumetric muscle defects could be restored after transplantation [12]. Although this strategy effectively facilitates tissue construction, the 3D printing method has limitations. In these systems, timing the interventions according to each cell's unique properties remains a challenge. However, there are still many challenges: (1) developing and refining methods for constructing functional biomimetic vasculature and skeletal muscle, (2) establishing a multicellular co-culturing system that supports self-assembly and differentiation capabilities, and (3) optimizing the timing of bioactive signals and nutrient supply to target cell types in a multicellular system. Developing new tissue engineering methods to construct vascularized skeletal muscle is critical.

This study examined temporal and spatial dynamics of the co-culture of multiple cells in skeletal muscle tissue, to construct vascularized muscle tissue with intricate structures. The results highlighted the effectiveness of the 3D demolding method and the influence of vascular network formation on muscle differentiation. Ultimately, 3D printing and precise timing adjustments can produce vascularized skeletal muscles with mature myotubes, setting the stage for future research on advanced muscle structures and multicellular systems.

Materials and methods

Cell culture

The mouse myoblast cell line C2C12 was obtained from the Shanghai Cell Bank of the Chinese Academy of Sciences. C2C12 cells were cultured in a proliferation medium (PM) consisting of Dulbecco's modified Eagle's medium (DMEM)—high glucose (C11965500BT, Gibco, Beijing, China), fetal bovine serum (FBS, 10% (0.1 g/mL); 10,099-141C, Gibco, Beijing, China), and penicillin/streptomycin (PS, 1% (0.01 g/mL); C11965500BT, Gibco, Beijing, China) for 2 days within 15 generations under 5% (0.05 g/mL) CO_2 at 37 °C. The human umbilical vein endothelial cells (HUVECs) and red fluorescent protein (RFP)-HUVECs were obtained from Prof. Lijian Hui's group (CAS Center for Excellence in Molecular Cell Science, China). The HUVECs and RFP-HUVECs were cultured on gelatin (0.1% (0.001 g/mL), G1890, Sigma, Beijing, China)-coated 10-cm cell culture petri dish in endothelial cell growth medium-2 (EGM-2, CC3162, Lonza, Shanghai, China) for 3 days within 14 generations under 5% CO_2 at 37 °C.

Bioink preparation

DMEM was dissolved in gelatin (G1890, Sigma, Beijing, China) at 37 °C for 1 h. Fibrinogen (F8630, Sigma, Beijing, China) was dissolved in sanitary water (BL100310) at 37 °C for 2 h. Thrombin (T4648-1KU, Sigma, Beijing, China) was dissolved in phosphate buffered saline (PBS). The C2C12 cell-laden bioink consisted of fibrinogen (20 mg/mL) and 5% (0.05 g/mL) gelatin at a concentration of 1×10^7 cells/mL. HUVECs were encapsulated in the mix of fibrinogen (10–20 mg/mL) and thrombin (2 U/mg) at a concentration of 5×10^6–1×10^7 cells/mL. The HUVECs containing cell hydrogel (fibrinogen/gelatin) mixture (HFG) consisted of fibrinogen (10–20 mg/mL), 5% (0.05 g/mL) gelatin, and thrombin (2 U/mg) at a concentration of 5×10^6–1×10^7 cells/mL.

3D printing of anchor and polydimethylsiloxane (PDMS) model

Overall, 5 g of the printed PDMS (SE1700, DOWSIL, Shanghai, China) stock solution and curing agent (stock solution:curing agent = 10:1) were mixed and defoamed, after which the mixture was poured into the printing cartridge and defoamed. The printing cartridge was installed on the 3D printer (Bio-Architect®-WS, Hangzhou, China). Bio Architect software was initiated before importing the model constructed in SolidWorks into the printer, and the printing speed, thickness, and number of layers were set. The printing pressure was maintained from 0.25 to 0.35 MPa, and the printing scaffold was started after the filament was smoothly tested. The struts constructed using a light-curing printer (Stratasys Object260 Connex3, Shanghai, China) were fixed to both ends of the PDMS frame and crosslinked at 60 °C for 4 h. The scaffolds were removed and sterilized.

The demolding model of the PDMS model was printed via Ultimaker. The PDMS (DKN1841100, Shanghai, China) stock solution (5 g) and curing agent (stock solution:curing agent = 10:1) were mixed and defoamed. The PDMS in the demolding model was added, the mold was degassed under vacuum for 30 min, and then, the PDMS mold was maintained at 40 °C for 24 h. The PDMS mold was removed and sterilized with ethylene oxide. The groove width parameter of the demolding model was modified according to the fascicle width (800–1200 μm).

3D bioprinting of muscle constructs

SIA Bioprinter PRO printer developed by the Shenyang Institute of Automation, Chinese Academy of Sciences, was used for 3D bioprinting. C2C12 cell-laden bioink was prepared and precooled at 4 °C for 10 min in a special SIA Bioprinter PRO barrel. The barrel was installed at the specified position,

and the temperature of the platform was adjusted to 6 °C. The temperature of the nozzle and needle was adjusted from 18 to 25 °C to ensure that the filament state was maintained in the gel state. The nozzle and base plate were calibrated. The end position of printing was set as the origin of printing, and the parameters were saved and downloaded. Then, the model constructed in advance was imported, the silk condition was tested, and the muscle bundle was printed.

In vitro culture of muscle bundles

The anchor was inserted into both ends of the printed construction and added thrombin (20 U/mg) was covered around the hydrogel, crosslinked at 25 °C for 45 min, and at 37 °C for 10 min. Muscle bundles were put into 6-well plates to culture with PM (2 mg/mL 6-aminocaproic acid (6-AA, A2504-25G, Sigma)) for 1 d. The differentiation medium (DM), which consisted of DMEM, 2% horse serum (HS, 26,050,088, Gibico, Beijing, China), 1% PS, 2 mg/mL 6-AA, and 1 μmol/mL insulin (I6634, Sigma), was changed daily.

Construction of vascularized muscle bundles

For the adhesion monolayer cell formation method, the 1-day differentiated muscle bundle (DM1) was placed into the PDMS mold, and then, HUVEC suspension, at a density of 5×10^6 cells/mL, was added to the groove until the muscle bundle was removed entirely at 37 °C for 30 min. The muscle bundle was turned over, and the cell suspension was replenished until completely unwashed at 37 °C for 30 min. The muscle bundles adhering to RFP-HUVECs were placed in 6-well plates, the 50% DM + 50% EGM-2 was added, and the medium was changed daily. The HFG wrapping method is as follows: The DM1, DM4, or DM7 muscle bundles were placed on the "three-in-one" mold, and HFG with HUVEC density of 5×10^6–1×10^7 cells/mL was added to the groove. The top cover was installed and placed at 37 °C for 6 min. The muscle bundles were removed from 6-well plates and co-cultured for 6 d, known as DM1+6, DM4+6, or DM7+6 groups. The medium was changed daily.

Rheological tests

The test samples were 5% gelatin–2% fibrinogen, 3.5% gelatin–2% fibrinogen, 5% gelatin, and 3.5% gelatin using a rotor of pp-25 mm (diameter). The shear thinning test conditions were as follows: The test temperature was 8 °C, the test strain was 1%, the shear rate ranged from 0.001–100 s^{-1}, and the sample was maintained at 8 °C for 5 min before starting the test. The temperature scan test conditions were as follows: The test temperature ranged from 4 to 40 °C, the test strain was 1%, the shear rate was 1%, and the test was started after holding at 40 °C for 5 min. The frequency scan test conditions were as follows: The test temperature was 8 °C, the test strain was 1%, the shear frequency ranged from 0.01 to 10 Hz, and the test was started after holding at 8 °C for 5 min. The test conditions for alternating strain changes were as follows: The test temperature was 8 °C, the strain change was 0.5% for 100 s, and then, the change was 500% for 100 s, alternating for six cycles, and the experiment was started after 5 min of insulation at 8 °C.

Cell viability tests

An appropriate volume of staining solution with 0.5 μL/mL calcein, 2 μL/mL ethidium bromide dimer, and Hoechst (1:1000) was added to the sample to ensure that the sample does not pass the model entirely. The staining condition was 37 °C in the dark for 30 min. The staining solution was discarded, the cells were washed once with PBS, the medium was added, and the sample was observed under a dragonfly microscope. Viable cells (green) versus dead cells (red) were counted using ImageJ software, and the cell viability was calculated by dividing the number of viable cells by the total number of cells ($n = 3$).

Histologic and immunofluorescence staining

The samples were fixed using 4% paraformaldehyde (PFA) (0.04 g/mL) for 24 h and washed thrice with PBS to prepare them for staining. The samples were routinely treated and embedded in paraffin. Transverse sections were placed on salinized slides for immunohistochemistry using platelet endothelial cell adhesion molecule-1 (CD31) (ab28364, Abcam, Shanghai, China). The other samples were fixed using 4% PFA for 24 h and washed thrice with PBS to prepare them for staining. The samples were thoroughly immersed in 1% (0.01 g/mL) Triton X-100 dissolved in PBS with permeable membrane solution, placed on a shaker, incubated for 2 h at 25 °C, and washed three times with PBS. The samples were then thoroughly soaked by adding 5% (0.05 g/mL) bovine serum albumin (BSA) solution and placed on a shaker overnight at 4 °C. Myosin heavy chain (MHC) antibody was diluted by 1:200 in the blocking solution, CD31 antibody was diluted at a ratio of 1:200, and VE-cadherin (VE–Cad) antibody was diluted at a ratio of 1:200 in the blocking solution. 4′,6-Diamidino-2-phenylindole (DAPI) was diluted 1:1000 on a shaker overnight at 4 °C. Then, 10 mL PBST (10 mL PBS + 10 μL Tween–20 (dope) + 10 μL Triton X-100 (dope))

was added three times (30 min each time). The secondary antibodies were diluted with PBST at a ratio of 1:500 and incubated for 2 h at room temperature under dark conditions. They were placed on a shaker at room temperature and washed thrice with PBST for 30 min each time. Staining results were observed using a confocal microscope or live cell workstation.

Quantitative reverse transcription polymerase chain reaction (RT-qPCR) analyses

The expression levels of mouse myogenic and vascularized genes in vascularized skeletal muscle were assessed via two-step RT-qPCR. After the vascularized skeletal muscle was differentiated and cultured up to Days 7, 10, and 13, the samples were removed, and 800 μL of TRIzol was added. RNA was extracted using glycogen (R0551, Thermo Fisher Scientific, USA) via standard methods, and RNA (1 μg) was reverse transcribed into cDNA using PrimeScript™ RT Master Mix (RR036A, TaKaRa, Shanghai, China); they were then diluted with RNase-free water. The expression levels of myogenic differentiation genes (*MyoD1*, *Myf5*, *MyoG*, *Myh1*, *Myh2*, *Myh4*, and *Myh7*) along with vascularization genes (*CD31*, *CD34*, *CD144*, and *vWF*) were analyzed using Hieff® qPCR SYBR Green Master (No Rox) (11201ES03, Yeasen, Shanghai, China). Glyceraldehyde-3-phosphate dehydrogenase (GAPDH) was used for internal standardization. Primers for RT-qPCR in this study are listed in Table S1 (Supplementary Information). Data analysis was conducted based on the following formula, where cDNA cycle threshold (C_t) values were derived from real-time PCR software, and were derived from the average C_t values of three samples:

(a) dC_t (sample, gene) = C_t (sample, gene) − average (C_t (sample, GAPDH)),
(b) ddC_t (sample, gene) = dC_t (sample, gene) − average ((dC_t (control, gene))),
(c) Foldchange = $2^{-ddC_t\,(\text{sample, gene})}$.

Statistical analyses

All data were presented as mean ± standard deviation. The *t*-test was used for statistically significant differences between groups. GraphPad Prism 8 (GraphPad Software, Inc.) was used for statistical analysis. Statistical significance was indicated as follows: $^{*}p < 0.05$, $^{**}p < 0.01$, $^{***}p < 0.001$, and $^{****}p < 0.0001$.

Results

Fabrication and characterization of the muscle bundle

In this study, we examined the rheological analysis of a hydrogel system comprising gelatin + fibrinogen (referred to as Gel–Fib hydrogel). Due to gelatin's thermosensitive nature, the phase transition point of 5.0% gelatin + 2.0% fibrinogen was observed at 22 °C (Fig. 1a). The viscosity of the materials used in the four groups of experiments decreased with the increase in shear rate, which has the property of shear thinning (Fig. 1b), so the damage to the cells would reduce when the printing needle extracts the material [19]. Additionally, the Gel−Fib hydrogel had strong mechanical properties, which could stack multi-layer hydrogel (Fig. S1a in Supplementary Information). Then, the ink was maintained in a printable state extruded from the needle by adjusting temperature (Fig. 1c). It was demonstrated that the state of the four materials could be maintained stable in the change cycle, indicating that gelatin and Gel–Fib could quickly recover after extrusion and were suitable for 3D printing (Fig. S1b in Supplementary Information). These results suggest that the Gel–Fib hydrogel has strong printing stability accompanied by characteristics of shear thinning, self-healing, and high modulus.

Skeletal muscle bundles were constructed according to the 3D bioprinting method. In this study, an H-shaped structure was developed via 3D bioprinting [16]. Scaffolds were installed at both ends to maintain the unidirectional force required for skeletal muscle differentiation (Figs. 1d1). Gel—Fib hydrogel was used as cell-loaded printing ink to print muscle bundles (with a size of 14 mm × 1 mm × 2 mm) on the slides (Figs. 1d2–1d4). After printing, the scaffolds constructed via 3D printing in advance were fixed to both ends of the printed muscle bundles and then crosslinked after dropping the thrombin. The width of the muscle bundle changed significantly at the beginning of the culture (Fig. S2 in Supplementary Information). Live/dead staining assay showed a great number of live cells, with a cell viability of 90% (Fig. 1f) when C2C12 cells were proliferated for 1 day to stably maintain their adherence to the hydrogel (Fig. 1h). It was shown that constructing muscle bundles via 3D bioprinting had less effect on C2C12 cells and contraction during the muscle bundles culture.

Myoblasts form multinucleated myotubes through migration, orientation, and membrane fusion [1]. Staining of the cytoskeleton showed that C2C12 cells showed exposure on Day 4 of differentiation, which became more evident on Day 7 of differentiation and culture (Fig. S3a in Supplementary Information). The orientation distribution ratio of cells showed that the orientation of cells increased significantly on Day 7 of fasciculation (Fig. S3b in Supplementary

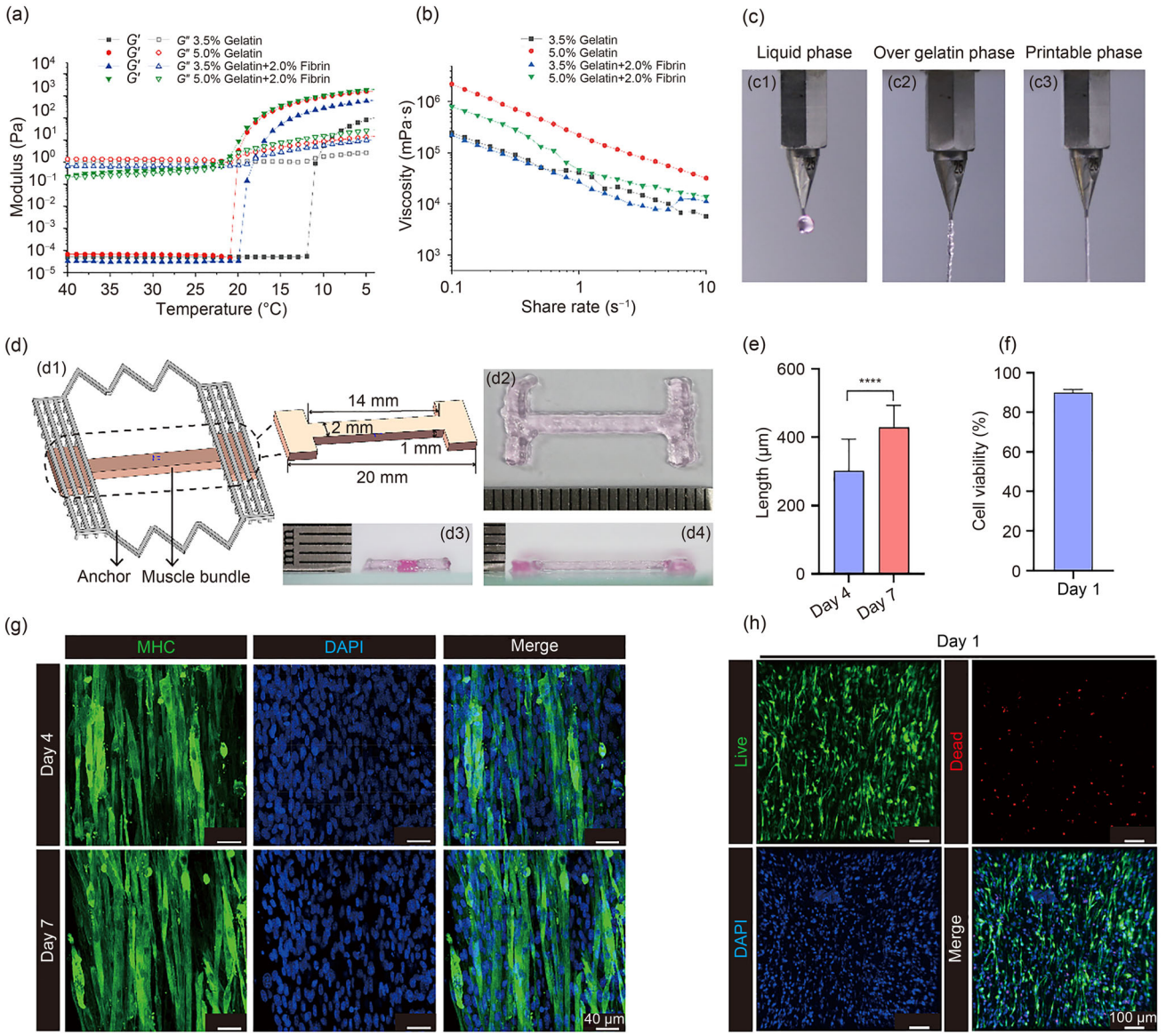

Fig. 1 Construction of the skeletal muscle via 3D printing. **a** Temperature across curves of gelation and gelation-fibrinogen (from 40 to 4 °C, 1 Hz, strain 1%). **b** The shear rate ranged from 0.1 to 10 s^{-1} across curves of gelation or fibrinogen (strain 1%, 8 °C). **c** Extrusion of 3.5% gelation + 2.0% fibrinogen shows the liquid, over gelation, and printable phases at different temperatures. **d** The schematic illustrations and optical images of construction, including the schematic illustrations of muscle bundle and PDMS anchor (d1), and aerial view, left view, and front view of printed construction (d2–d4). **e** The length of the muscle tube calculated on Days 4 and 7 ($^{****}p < 0.0001$, $n = 3$). **f** Myoblast cell viability after 1-day proliferation ($n = 3$). **g** Immunolabeling for MHC (green) with Hoechst counterstain for assessing the degree of myogenic differentiation on Days 4 and 7. **h** Live (green)/dead (red) staining after 1 day. PDMS: polydimethylsiloxane; MHC: myosin heavy chain; DAPI: 4′,6-diamidino-2-phenylindole

Information). Therefore, myoblasts are gradually oriented and arranged following the process of differentiation and culture. The formation of myotubes in muscle bundles was observed via immunofluorescence staining. It was demonstrated that shorter primary myotubes were formed on Day 4 and that myotubes continued to fuse to form longer secondary myotubes on Day 7 during the differentiation process of muscle fasciculus (Fig. 1g and Video S1 in Supplementary Information). The myotubes length measured by ImageJ showed a significant increase in myotubes length on Day 7 (Fig. 1e). Myoblasts fused to longer multinucleated myotubes during the differentiation of muscle bundles.

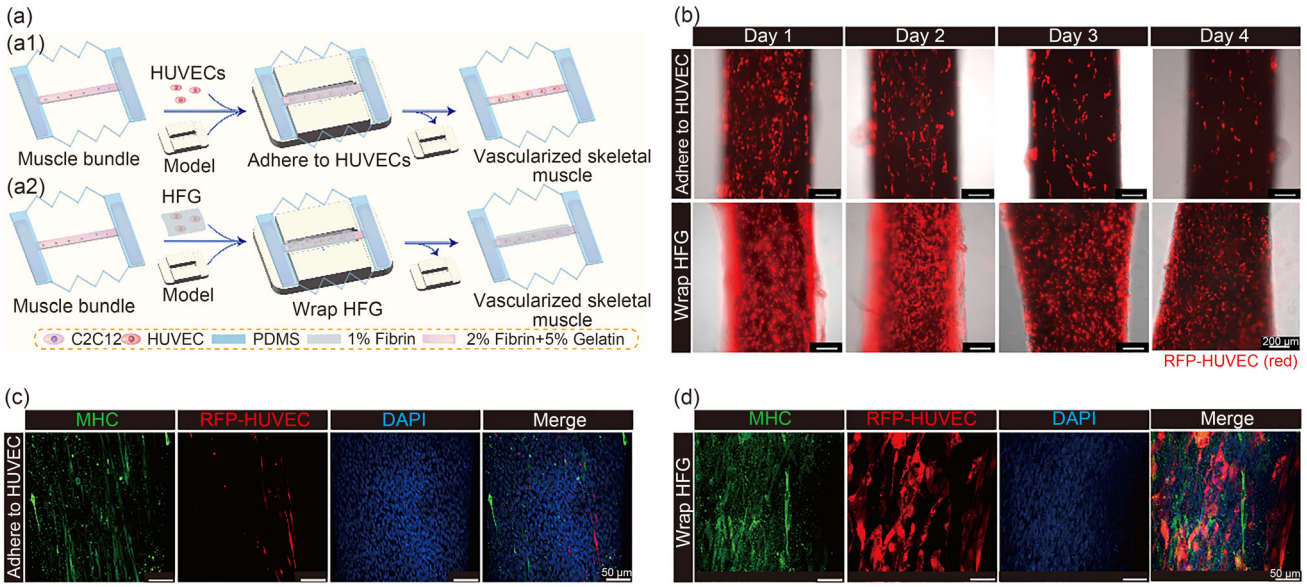

Fig. 2 Evaluation of the mechanism of constructing vascularized skeletal muscle. **a** Schematic illustration of adhering HUVECs to the muscle bundle (a1) and wrapping the HFG outside the muscle bundle via 3D printing (a2). **b** HUVEC (red) adhesion observed continuously via microscopy of the muscle bundle for 4 days. **c** Immunolabeling for MHC (green) with Hoechst and RFP-HUVEC for assessing the degree of myogenic differentiation and self-assembling of HUVECs on Day 7. **d** The state of HUVEC (red) maintenance of muscle fiber observed continuously via microscopy for 7 days. HUVEC: human umbilical vein endothelial cell; RFP: red fluorescent protein; MHC: myosin heavy chain; DAPI: 4′,6-diamidino-2-phenylindole; HFG: HUVECs containing cell hydrogel (fibrinogen/gelatin) mixture; PDMS: polydimethylsiloxane

Construction of vascularized skeletal muscle with HUVECs wrapped outside the muscle bundle

The vascular network was constructed as thin as possible to build a more bionic vascularized skeletal muscle and satisfy the 200-μm nutrient delivery restriction [20]. We designed two construction strategies to construct the vascular network: Fig. 2a1 shows monolayer HUVECs adhering outside the muscle bundle during differentiation, and Fig. 2a2 shows the HFG wrapping around the muscle bundles at stages of differentiation.

HUVECs can be achieved equably outside the muscle bundle on the 1st day of differentiation (Fig. S4a in Supplementary Information). However, HUVECs gradually fall off during differentiation and culture, and the density of HUVECs could not satisfy the formation of vascular networks on Day 4 (Fig. 2b). HUVECs adhere outside the muscle bundles to differentiate for 3 days. A high density of HUVECs could conform to the outside of the muscle bundles, which differentiated up to 1–3 days (DM1–DM3) (Fig. S4a in Supplementary Information). HUVECs were gradually shed from muscle bundles in the three groups during 3 days of continuous culture (Fig. S4b in Supplementary Information). The results showed that the change in muscle bundle volume affected the adhesion of HUVECs. Therefore, the adhesion methods that facilitate the adherence of HUVECs outside the muscle bundle could not achieve the construction of vascularized skeletal muscles.

Wrapping HFG was used to construct vascularized skeletal muscles, and the hydrogel provided a growth space for HUVECs to maintain the long-term culture outside the fascicle. Adherent HUVECs could not achieve the differentiation of myotubes outside the muscle bundle (Fig. 2c). Wrapping HFG outside the muscle bundle showed that HUVECs could adhere around the muscle bundle for 4 days and began to extend (Fig. 2b). It was indicated that the viability of HUVECs was >90% after 1 day of culture in 1% and 2% fibrin for a 3D culture (Fig. S5 in Supplementary Information). HUVEC encapsulation was evident on the outside of the bundle after 7 days of differentiation, and myotubes appeared within the entire bundle (Fig. 2d). Therefore, this method can initially achieve the construction of vascular skeletal muscle with blood vessels and multinucleated myotubes.

PDMS release mold was used to wrap hydrogel outside the muscle bundle, which is known as a “three-in-one” mold (Fig. 3a). The operation of PDMS to wrap the hydrogel into a muscle bundle is more suitable due to the soft material of PDMS [21], which can be easily removed from the mold because PDMS has strong hydrophobicity and less adhesion to fibrin [22].

HUVECs mixed with 2% fibrin coated outside the DM1 muscle bundle showed poor extension on Day 3 (Fig. S6 in

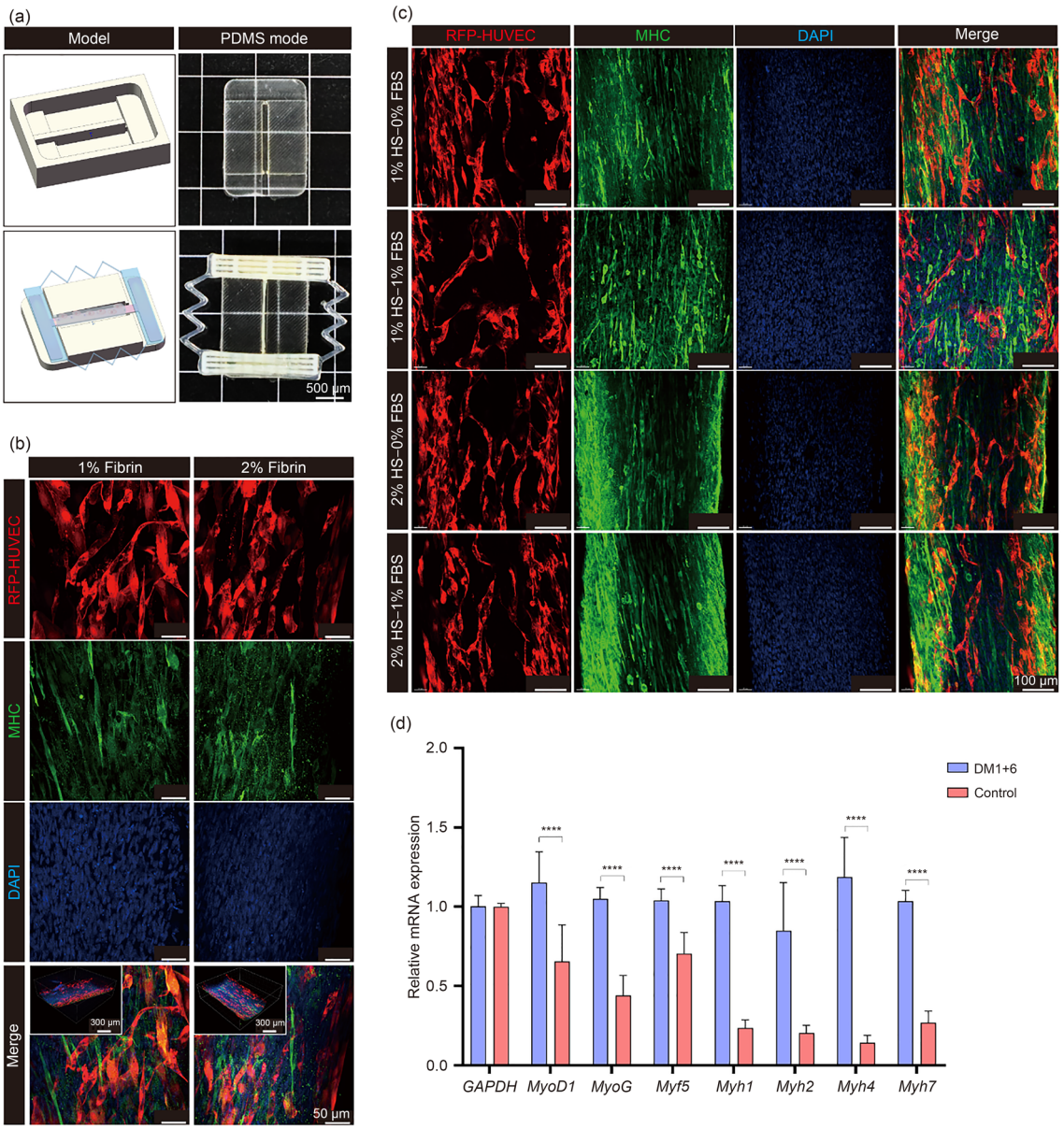

Fig. 3 Optimization of constructing vascularized skeletal muscle to the culture. **a** The demolding model and working illustration of the PDMS mold. **b** The DM1 muscle bundles wrapped with 1% and 2% fibrin and cultured to Day 7 (DM1+6) (HUVEC (red), MHC (green), and DAPI (blue)). **c** Culture of DM1 muscle bundles which wrapped 1% HFG using four types of media (HS–FBS), and observation of the fusion of myotubes (MHC, green) and self-assembling of HUVECs (red) (DAPI, blue). **d** The expression levels of C2C12 differentiated myogenic marker genes (*MyoD1*, *MyoG*, *Myf5*, *Myh1*, *Myh2*, *Myh4*, and *Myh7*) in vascularized skeletal muscle were analyzed via quantitative PCR in DM1+6 and control groups ($^{****}p < 0.0001$, $n = 3$). MHC: myosin heavy chain; DAPI: 4′,6-diamidino-2-phenylindole; PDMS: polydimethylsiloxane; HS: horse serum; FBS: fetal bovine serum; HUVEC: human umbilical vein endothelial cell; DM: differentiation medium; PCR: polymerase chain reaction; RFP: red fluorescent protein

Supplementary Information). It was observed that the vascularization was not obvious, and almost no myotubes formed over 7 days. HUVECs showed an evident stretching phenomenon on Day 3 in the 1% fibrin group; the vascularization could be observed over 7 days of differentiation, and primary myotubes could be noted inside the muscle bundles (Fig. 3b).

We screened the co-culture medium to form the vascular network and dense secondary myotubes to achieve the codifferentiation of HUVECs and C2C12 cells in vascularized skeletal muscle. HUVECs had high viability and could extend after culturing for 3 days with various concentrations of HS and FBS (Fig. S7 in Supplementary Information).

Next, we used the same medium formulation for differentiated vascularized skeletal muscle tissue cultures. HUVEC self-assembly and vascularization are more pronounced at 1% FBS concentrations in the DM1+6 group (Fig. 3c). Multinucleated myotubes appeared when HS concentration was increased to 2%.

The myogenic differentiation of vascularized and non-vascularized muscle bundles in the same medium (2% HS–1% FBS) was analyzed by RT-qPCR. The mRNA expression levels of *MyoD1*, *MyoG*, *Myf5*, *Myh1*, *Myh2*, *Myh4*, and *Myh7* in the vascularized muscle bundles (DM1+6) were higher than those in the non-vascularized muscle bundles (Fig. 3d). This indicated that the construction of a vascular networks can promote the differentiation and maturation of myotubes.

The time of vascular network construction affects myotube differentiation

To explore the effect of differences in vascularization time on vascular and skeletal muscle, we use the "three-in-one" mold to wrap HFG outside the muscle bundles on Days 1, 4, and 7 during the differentiation period, referred to as DM1, DM4, and DM7, respectively (Fig. 4a). Hydrogel with the thickness of about 100 μm was surrounded outside the muscle bundles on different days of differentiation (Fig. 4e) and the width of the muscle bundle was decreased during the differentiation (Fig. 4d). The DM1, DM4, and DM7 muscle bundles encapsulated with HFG differentiated over 3 days. HUVECs gradually extended, and almost no cells were shed during the culture period (Fig. S8 in Supplementary Information). HUVECs showed an apparent extension phenomenon and uniform distribution on Day 6 of differentiation, achieving a long-term culture of HUVECs (Fig. 4b).

To explore the effect of vascular network construction time on myotubes differentiation, we investigated the effect of vascular network construction by muscle bundles differentiated into different stages and found that myotubes and vascular networks were formed in all three groups (Fig. 4c and Video S2 in Supplementary Information). The myotubes were shorter in the DM1+6 group, and most of them were primary myotubes with two nuclei. In the DM4+6 group, longer myotubes with three nuclei (about 200 μm) appeared. However, in the DM7+6 group, the myotubes grew to about 350 μm, with about five nuclei in a single myotube and longer secondary myotube (Figs. 4g and 4h). There was no significant difference in the width of the myotubes among the three groups (Fig. 4h). The appearance of multinucleated myotubes is a vital indicator of the maturity of myoblasts [23]. The number of nuclei in the DM7+6 group was the highest. Therefore, on Day 7 of muscle bundle differentiation, HUVECs were added to construct vascularized skeletal muscle, longer myotubes could be formed, and the muscle bundle was more mature.

The expression of CD31 and VE–Cad was observed in DM1+6, DM4+6, and DM7+6 groups, indicating a tight junction presented between HUVECs and the cells that occurred endothelialization [24]. The self-assembly state of HUVECs showed that there were tube network connections and myotube formation (Fig. 5a; Fig. S9 and Video S3 in Supplementary Information). To verify the degree of myogenic differentiation and vascularization at the molecular level, the differentiation genes *MyoD1*, *MyoG*, *Myf5*, *Myh1*, *Myh2*, *Myh4*, and *Myh7* of C2C12 cells were detected by RT-qPCR (Figs. 5b–5h). The expression of *MyoD1* in the DM4+6 group was higher than that in the DM1+6 group, indicating that most of the myoblasts in the DM4+6 group were in the stage of monocytic differentiation. Moreover, the expression levels of *Myh1*, *Myh2*, *Myh4*, and *Myh7* in the DM7+6 group were higher than those in the other two groups, indicating that most of the myoblasts in the DM7+6 group were in the stage of multinucleated differentiation [25], which again verified that the degree of differentiation of the DM7+6 group was higher.

Discussion

Existing vascularized skeletal muscle methods can construct vascularized structures with muscle tubes, but there are still problems such as poor biomimetic degree [4, 17]. We intervened in the vascularization process to increase the complexity and biomimetic degree of skeletal muscle tissue construction through 3D printing and 3D modeling. This was performed to achieve the structure of vascularized skeletal muscle that can regulate the vascularization process and myotubes in both time and space.

3D printing is a state-of-the-art technology as it allows rapid and precise construction of individual geometries according to different requirements [15]. Moreover, its printing accuracy is high, which ensures that the PDMS mold can adjust the size according to the width of the muscle bundle to ensure that the thickness of HFG is uniform. Compared with unprinted structures, 3D bioprinting can premodulate the arrangement of cells in the constructed muscle bundles showing a more pronounced orientation [16, 26]. Therefore, it can arrange living cells with biomaterials to generate specified three-dimensional structures by jetting or extrusion, constructing tissues with intact structures that can be transplanted in vitro [15]. We selected gelatin and fibrinogen as printing inks owing to their mechanical properties, rheological properties, biological activity, and biocompatibility [27–32].

The vascular network wrapped around the muscle bundle has a topology that is like the physiological structure and

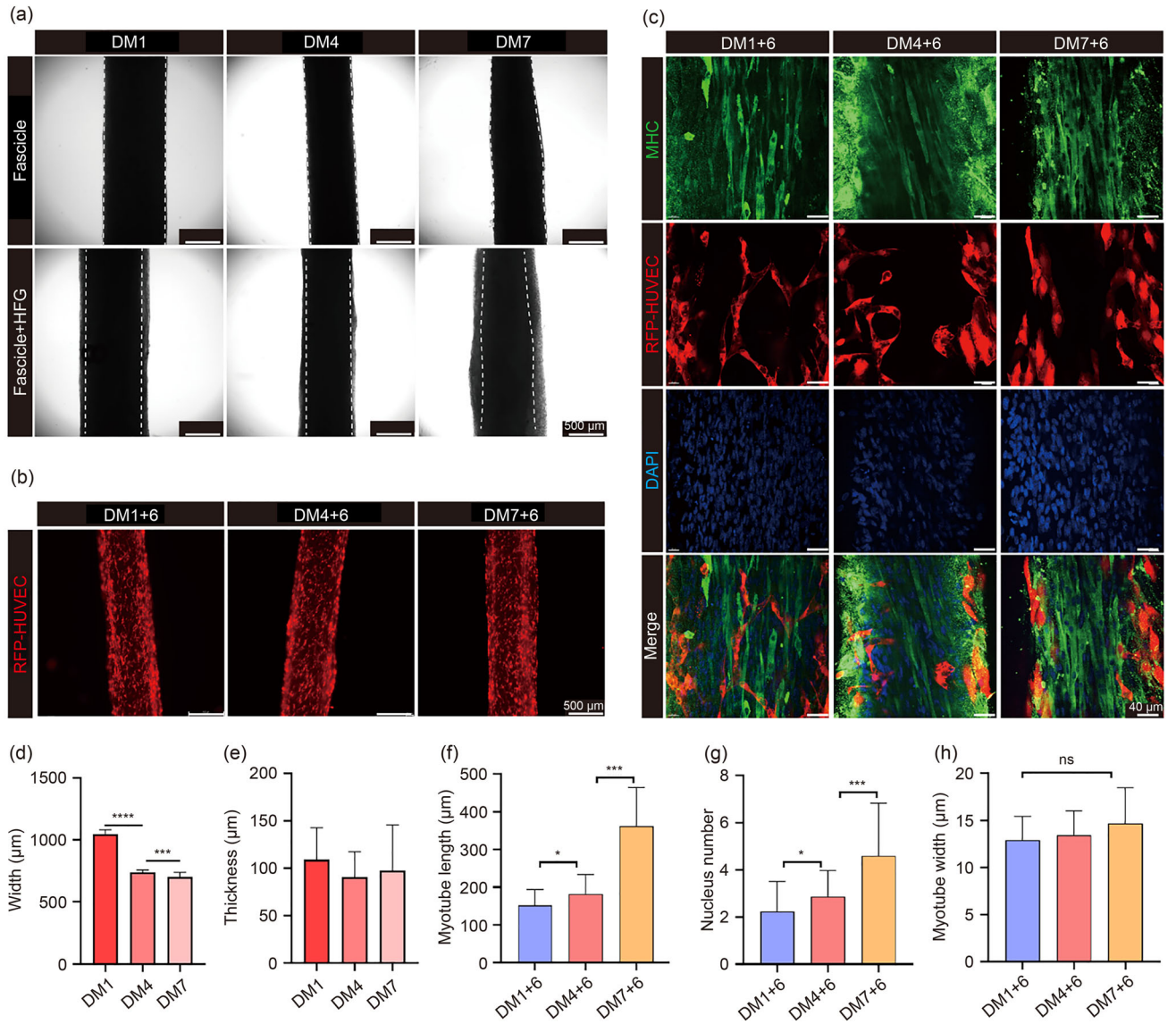

Fig. 4 Construction of vascularized skeletal muscle by wrapping HFG to muscle bundles at different days of differentiation. **a** Light microscopic observation of wrapping HFG at 1-, 4-, and 7-day differentiation. **b** Fluorescence microscope observation of 1-, 4-, and 7-day differentiated muscle bundles with HUVECs (red) cultured for 6 days. **c** Observation of fusion of myotubes (MHC, green) and self-assembling of HUVECs (red) by wrapping HFG to muscle bundles at different days of differentiation. **d** The width of muscle bundles measured in 1-, 4-, and 7-day differentiation. **e** The thickness of HFG outside the muscle bundles. **f**–**h** Quantitative statistics of myotube length, nucleus, and width of DM1+6, DM4+6, and DM7+6. $^{*}p < 0.5$, $^{***}p < 0.001$, $^{****}p < 0.0001$, $n = 3$. HUVEC: human umbilical vein endothelial cell; RFP: red fluorescent protein; MHC: myosin heavy chain; DAPI: 4′,6-diamidino-2-phenylindole; HFG: HUVECs-containing cell hydrogel (fibrinogen/gelatin) mixture; DM: differentiation medium; ns: not significant

is more biomimetic. Compared with the naturally occurring arrangement of adipocytes (fat cells) and blood vessels within macroscopic skeletal muscle, and the design of arterioles and venules accompanying muscle fascicles, the arterial and venous networks, when constructed separately, cannot adequately perfuse the muscular structure with a width of 5 mm due to limitations in nutrient supply capacity [13, 33]. However, our goal was to engineer a highly organized vascular network that mirrors the dense capillary beds found in terminal arterioles, venules, and microvascular units, to achieve sufficient nutrient delivery throughout the entire muscle tissue. Additionally, the culture method of extra vascularizing HFG in the differentiation process can realize the time regulation of vascularization and the selection of the time point of co-culture between blood vessels and myotubes. This methodology can be used as a tissue model to investigate the relationships between myotubes and vascularization.

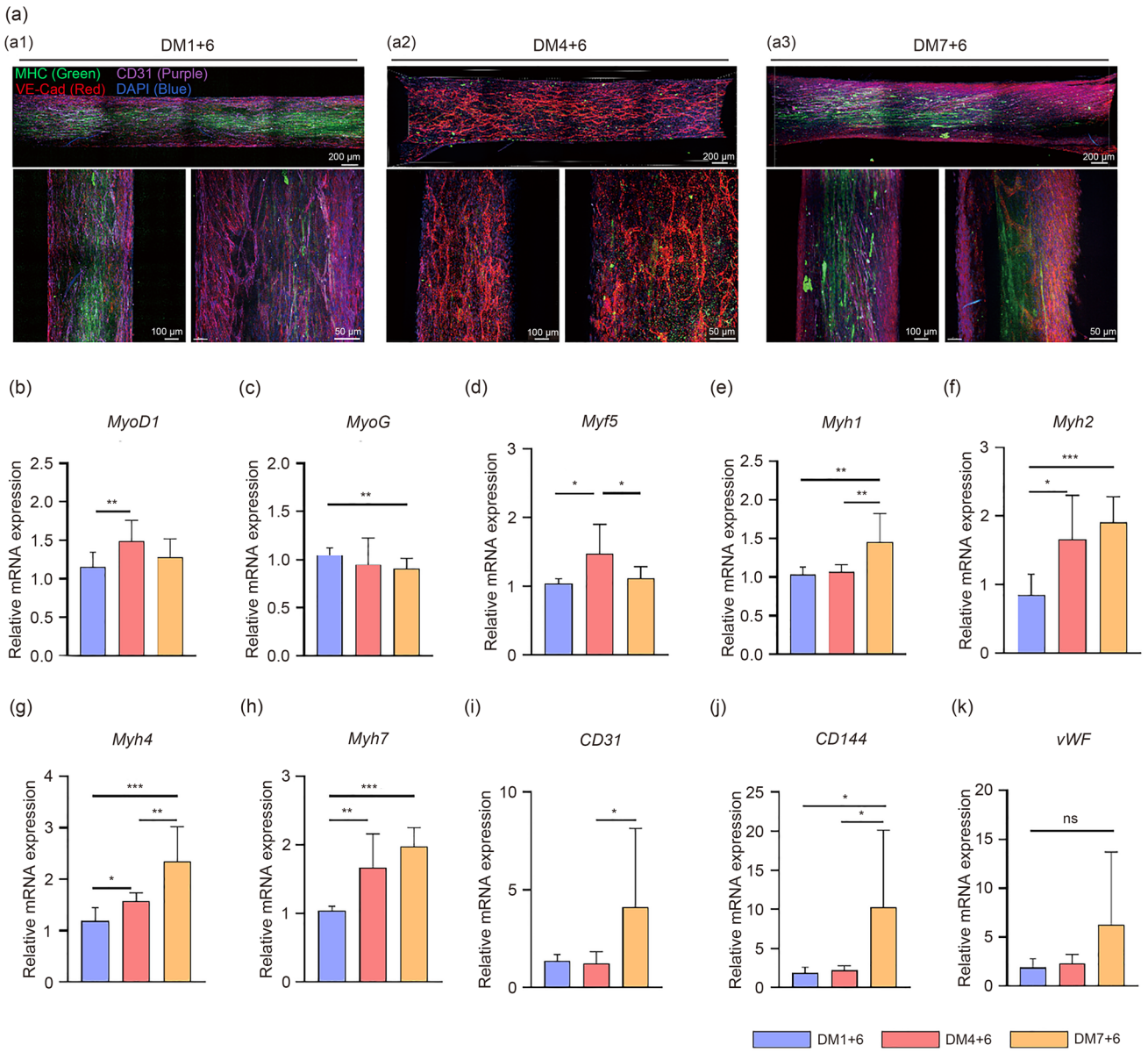

Fig. 5 Differentiation of myotubes and blood vessel formation in vascularized skeletal muscles. **a** HFG was outsourced to muscle bundles for 1, 4, and 7 days, followed by a 6-day vascularization construction period to observe the differentiation of muscle tubes and blood vessels. (a1–a3) Fasciculation culture for 1-, 4-, and 7-day-wrapped HFG was recorded as DM1+6, DM4+6, and DM7+6, respectively (CD31 (purple), VE—Cad (red), MHC (green), DAPI (nucleus, blue)). **b–h** The expression levels of C2C12 differentiated myogenic marker genes (*MyoD1*, *MyoG*, *Myf5*, *Myh1*, *Myh2*, *Myh4,* and *Myh7*) in vascularized skeletal muscle were analyzed by qPCR in DM1+6, DM4+6, and DM7+6 groups ($^{*}p < 0.05$, $^{**}p < 0.01$, $^{***}p < 0.001$, $n = 3$). **i–k** The expression levels of marker genes (*CD31*, *CD144*, and *vWF*) of HUVEC vascularization in vascularized skeletal muscle analyzed by qPCR in DM1+6, DM4+6, and DM7+6 groups ($p > 0.05$, $^{*}p < 0.05$, $n = 3$). VE–Cad: VE-cadherin; MHC: myosin heavy chain; DAPI: 4′,6-diamidino-2-phenylindole; DM: differentiation medium; HUVEC: human umbilical vein endothelial cell; HFG: HUVECs-containing cell hydrogel (fibrinogen/gelatin) mixture; qPCR: quantitative polymerase chain reaction

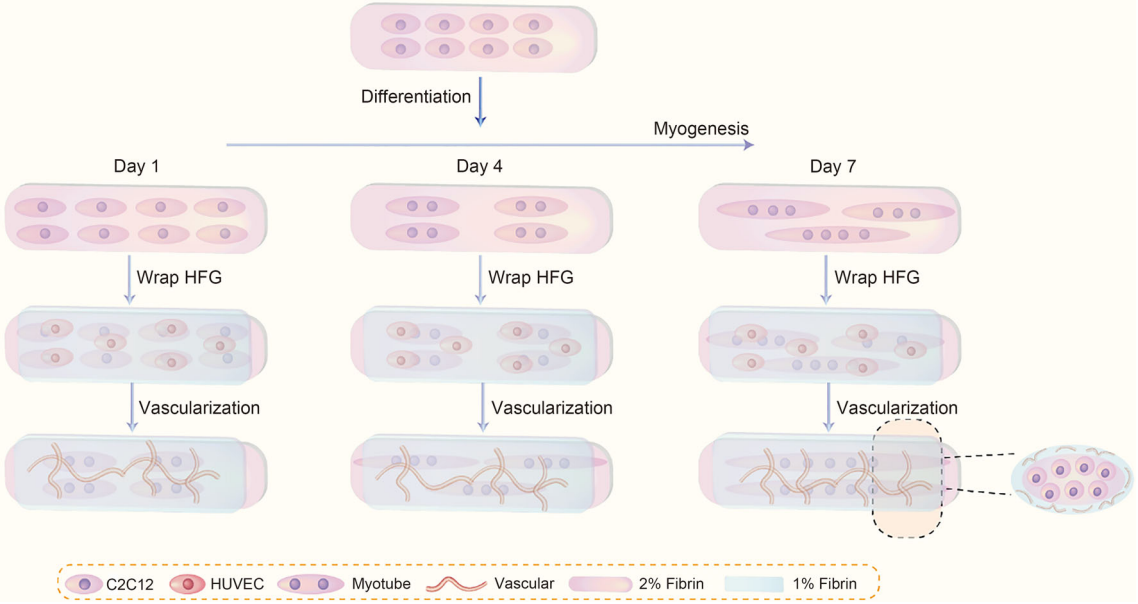

Fig. 6 The differentiation process of the vascularized skeletal muscle. The angiogenic genes *CD31*, *CD34*, *CD144*, and *vWF* in HUVECs were detected. Compared with the DM1+6 group, the DM7+6 group had higher expression of platelet endothelial cell adhesion molecule (CD31), hematopoietic stem cell marker (CD34), and VE–Cad (CD144), indicating more mature vascularization [35–37]. HUVEC: human umbilical vein endothelial cell; HFG: HUVECs-containing cell hydrogel (fibrinogen/gelatin) mixture; DM: differentiation medium

In vascularized skeletal muscle tissue, C2C12 cells and HUVECs have different requirements for differentiation [34]. It is impossible to coordinate the differentiation conditions between the two types of cells during co-culture to achieve a structure with mature vascularization and myotubes when regulating the onset time of vascularization. By comparing the expression of the vascularization marker CD31 with the myotube marker MHC at the molecular level, it is conducive to forming a more mature myotube structure after 7 days of differentiation [24]. Higher expression of vascularization marker genes can be observed at the molecular level when the vascular network is initiated later point. In summary, when the vascular network is created, an EGM-2 medium must be added to maintain the survival and differentiation of HUVECs and keep the cells in a high-proliferation environment. However, the medium used for C2C12 differentiation was HS, a differentiation environment devoid of proliferative factors, which inhibits the differentiation of C2C12 and significantly slows down the process of myotube formation [8]. We revealed that after C2C12 differentiated to form myotubes, and will maintain the current state.

We artificially regulated the construction of vascular networks at various stages of fascicular differentiation to regulate the initiation time and differentiation process of co-culture of the two types of cells. The vascular network starts when the fascicle is in the mononuclear differentiation period, resulting in the C2C12 always maintaining a low differentiation level in the muscle bundle. However, when C2C12 was in the early stage of multinuclear differentiation, a vascular network was established, and obvious multinuclear myotubes were observed inside the muscle bundle, although the maturity was subpar. When C2C12 was in the middle and late stages of multinuclear differentiation, the vascular networks began to be constructed, and it could be seen that there would be mature myotubes and more evident vascular networks (Fig. 6). Therefore, initiating vascular network construction after the formation of secondary myotubes is an approach to promoting the construction of in vitro vascularized skeletal muscle that maximizes the maturity of the internal structure of the tissue.

Conclusions

In this study, we constructed skeletal muscle using 3D bioprinting technology, complemented by the creation of a vascular network through 3D modeling technology. By modulating the interaction modes and timing between endothelial and muscle cells as well as using techniques such as immunofluorescence staining and RT-qPCR detection, we demonstrated that establishing the vascular network during the later stages of muscle bundle differentiation is beneficial for the formation of muscle tubes. This method, involving the regulated introduction of medium and sequential insertion of cells, was more effective for the co-culture of endothelial cells and myoblasts in our system. The method

also opens avenues for further exploration of the interplay between muscle bundle development and vascularization. However, the vascularized outer layer did not fully penetrate the inner skeletal muscle tissue to provide oxygen and nutrients, highlighting the ongoing challenges in fabricating bionic multicellular tissues.

Supplementary Information The online version contains supplementary material available at https://doi.org/10.1007/s42242-024-00315-0.

Acknowledgements The authors acknowledge the funding support from the National Natural Science Foundation of China (Nos. T2222029, U21A20396, and 62127811), the Strategic Priority Research Program of the Chinese Academy of Sciences (CAS) (No. XDA16020802), and the CAS Project for Young Scientists in Basic Research (No. YSBR-012). The authors also acknowledge the imaging technical support from Shiwen Li, Guoli Hou, and Xili Zhu of the CAS Imaging Platform.

Author contributions QG designed the experiments, supervised the work, and revised the manuscript. MXJ, TTF, and TJ performed the experiments and analyzed the results. MXJ wrote and revised the manuscript. XL and HL discussed the results and prepared the manuscript.

Declarations

Conflict of interest The authors declare that they have no conflict of interest.

Ethical approval This article does not contain any studies with human or animal subjects performed by any of the authors.

References

1. Frontera WR, Ochala J (2015) Skeletal muscle: a brief review of structure and function. Calcif Tissue Int 96(3):183–195. https://doi.org/10.1007/s00223-014-9915-y
2. Gillies AR, Lieber RL (2011) Structure and function of the skeletal muscle extracellular matrix. Muscle Nerve 44(3):318–331. https://doi.org/10.1002/mus.22094
3. Dziedzic D, Bogacka U, Ciszek B (2014) Anatomy of sartorius muscle. Folia Morphol 73(3):359–362. https://doi.org/10.5603/fm.2014.0037
4. Olfert IM, Baum O, Hellsten Y et al (2016) Advances and challenges in skeletal muscle angiogenesis. Am J Physiol-Heart C 310(3):H326-H336. https://doi.org/10.1152/ajpheart.00635.2015
5. Gholobova D, Terrie L, Gerard M et al (2020) Vascularization of tissue-engineered skeletal muscle constructs. Biomaterials 235:119708. https://doi.org/10.1016/j.biomaterials.2019.119708
6. Granger DN, Senchenkova E (2010) Inflammation and the microcirculation. Colloquium Ser Integr Syst Physiol 2(1):1–87. https://doi.org/10.4199/C00013ED1V01Y201006ISP008
7. Moriscot A, Miyabara EH, Langeani B et al (2021) Firearms-related skeletal muscle trauma: pathophysiology and novel approaches for regeneration. npj Regen Med 6(1):17. https://doi.org/10.1038/s41536-021-00127-1
8. Osaki T, Sivathanu V, Kamm RD (2018) Crosstalk between developing vasculature and optogenetically engineered skeletal muscle improves muscle contraction and angiogenesis. Biomaterials 156:65–76. https://doi.org/10.1016/j.biomaterials.2017.11.041
9. Corona BT, Rivera JC, Owens JG et al (2015) Volumetric muscle loss leads to permanent disability following extremity trauma. J Rehabil Res Dev 52(7):785–792. https://doi.org/10.1682/jrrd.2014.07.0165
10. Stevanovic M, Sharpe F (2014) Functional free muscle transfer for upper extremity reconstruction. Plast Reconstr Surg 134(2):257e–274e. https://doi.org/10.1097/PRS.0000000000000405
11. Zhuang P, An J, Chua CK et al (2020) Bioprinting of 3D in vitro skeletal muscle models: a review. Mater Des 193:108794. https://doi.org/10.1016/j.matdes.2020.108794
12. Choi YJ, Jun YJ, Kim DY et al (2019) A 3D cell printed muscle construct with tissue-derived bioink for the treatment of volumetric muscle loss. Biomaterials 206:160–169. https://doi.org/10.1016/j.biomaterials.2019.03.036
13. Gilbert-Honick J, Grayson W (2020) Vascularized and innervated skeletal muscle tissue engineering. Adv Healthc Mater 9(1):e1900626. https://doi.org/10.1002/adhm.201900626
14. Beldjilali-Labro M, Garcia AG, Farhat F et al (2018) Biomaterials in tendon and skeletal muscle tissue engineering: current trends and challenges. Materials 11(7):1116. https://doi.org/10.3390/ma11071116
15. Kang HW, Lee SJ, Ko IK et al (2016) A 3D bioprinting system to produce human-scale tissue constructs with structural integrity. Nat Biotechnol 34(3):312–319. https://doi.org/10.1038/nbt.3413
16. Fan TT, Wang S, Jiang ZM et al (2021) Controllable assembly of skeletal muscle-like bundles through 3D bioprinting. Biofabrication 14(1):015009. https://doi.org/10.1088/1758-5090/ac3aca
17. Gilbert-Honick J, Iyer SR, Somers SM et al (2018) Engineering functional and histological regeneration of vascularized skeletal muscle. Biomaterials 164:70–79. https://doi.org/10.1016/j.biomaterials.2018.02.006
18. Pinton L, Khedr M, Lionello VM et al (2023) 3D human induced pluripotent stem cell-derived bioengineered skeletal muscles for tissue, disease and therapy modeling. Nat Protoc 18(4):1337–1376. https://doi.org/10.1038/s41596-022-00790-8
19. Garcia-Cruz MR, Postma A, Frith JE et al (2021) Printability and bio-functionality of a shear thinning methacrylated xanthan-gelatin composite bioink. Biofabrication 13(3):35032. https://doi.org/10.1088/1758-5090/abec2d
20. Laschke MW, Harder Y, Amon M et al (2006) Angiogenesis in tissue engineering: breathing life into constructed tissue substitutes. Tissue Eng 12(8):2093–2104. https://doi.org/10.1089/ten.2006.12.2093
21. Miranda I, Souza A, Sousa P et al (2021) Properties and applications of PDMS for biomedical engineering: a review. J Funct Biomater 13(1):2. https://doi.org/10.3390/jfb13010002
22. Gokaltun A, Yarmush ML, Asatekin A et al (2017) Recent advances in nonbiofouling PDMS surface modification strategies applicable to microfluidic technology. Technology 5(1):1–12. https://doi.org/10.1142/s2339547817300013
23. Schmidt M, Schuler SC, Huttner SS et al (2019) Adult stem cells at work: regenerating skeletal muscle. Cell Mol Life Sci 76(13):2559–2570. https://doi.org/10.1007/s00018-019-03093-6
24. Bersini S, Yazdi IK, Talo G et al (2016) Cell-microenvironment interactions and architectures in microvascular systems. Biotechnol Adv 34(6):1113–1130. https://doi.org/10.1016/j.biotechadv.2016.07.002
25. Chal J, Pourquie O (2017) Making muscle: skeletal myogenesis in vivo and in vitro. Development 144(12):2104–2122. https://doi.org/10.1242/dev.151035
26. Kim JH, Seol YJ, Ko IK et al (2018) 3D bioprinted human skeletal muscle constructs for muscle function restoration. Sci Rep 8(1):12307. https://doi.org/10.1038/s41598-018-29968-5
27. Distler T, Solisito AA, Schneidereit D et al (2020) 3D printed oxidized alginate-gelatin bioink guides C2C12 muscle precursor cell

orientation and differentiation via shear stress during bioprinting. Biofabrication 12(4):045005. https://doi.org/10.1088/1758-5090/ab98e4
28. Kaczmarek B, Nadolna K, Owczarek A (2020) The physical and chemical properties of hydrogels based on natural polymers. In: Chen Y (Ed.), Hydrogels Based on Natural Polymers. Elsevier, Amsterdam, p.151–172. https://doi.org/10.1016/B978-0-12-816421-1.00006-9
29. Kolesky DB, Truby RL, Gladman AS et al (2014) 3D bioprinting of vascularized, heterogeneous cell-laden tissue constructs. Adv Mater 26(19):3124–3130. https://doi.org/10.1002/adma.201305506
30. Yu J, Wang K, Fan CC et al (2021) An ultrasoft self-fused supramolecular polymer hydrogel for completely preventing postoperative tissue adhesion. Adv Mater 33(16):e2008395. https://doi.org/10.1002/adma.202008395
31. Saroia J, Yanen W, Wei QH et al (2018) A review on biocompatibility nature of hydrogels with 3D printing techniques, tissue engineering application and its future prospective. Bio-Des Manuf 1(4):265–279. https://doi.org/10.1007/s42242-018-0029-7
32. Dietrich M, Heselhaus J, Wozniak J et al (2013) Fibrin-based tissue engineering: comparison of different methods of autologous fibrinogen isolation. Tissue Eng Part C 19(3):216–226. https://doi.org/10.1089/ten.tec.2011.0473
33. Kang DH, Louis F, Liu H et al (2021) Engineered whole cut meat-like tissue by the assembly of cell fibers using tendon-gel integrated bioprinting. Nat Commun 12(1):5059. https://doi.org/10.1038/s41467-021-25236-9
34. Jain RK, Au P, Tam J et al (2005) Engineering vascularized tissue. Nat Biotechnol 23(7):821–830. https://doi.org/10.1038/nbt0705-821
35. Dejana E, Orsenigo F (2013) Endothelial adherens junctions at a glance. J Cell Sci 126(12):2545–2549. https://doi.org/10.1242/jcs.124529
36. Sidney LE, Branch MJ, Dunphy SE et al (2014) Concise review: evidence for CD34 as a standard marker for diverse progenitors. Stem Cells 32(6):1380–1389. https://doi.org/10.1002/stem.1661
37. Lertkiatmongkol P, Liao DY, Mei H et al (2016) Endothelial functions of platelet/endothelial cell adhesion molecule-1 (CD31). Curr Opin Hematol 23(3):253–259. https://doi.org/10.1097/moh.0000000000000239